High Bandwidth Force Control for Robotic Friction Stir Welding

Valentin Kamm, Armin Lechler and Alexander Verl
Institute for Control Engineering of Machine Tools and Manufacturing Units
University of Stuttgart
Stuttgart, Germany
valentin.kamm@isw.uni-stuttgart.de

***Abstract*—Due to their flexibility and cost efficiency, industrial robots are increasingly being used for manufacturing processes. One such process is friction stir welding, which places high demands on the manipulator due to the high process forces and force gradients involved. The high compliance of industrial robots compared to traditional machine tools necessitates the implementation of force control for robotic friction stir welding. This paper presents an approach to increasing the bandwidth during force control of robotic friction stir welding. To achieve this, an industrial robot is controlled through an open control architecture, which offers the possibility to employ advanced force control structures. An admittance controller with inner velocity loop and a parallel force controller are compared to the state-of-the-art external force controller and validated in a digital twin of the robot. The most promising structure of the admittance controller is then implemented and validated on the test system, demonstrating an increase in accuracy and efficiency.**

***Index Terms*—Industrial robots, Control systems, Force control, Welding**

I. Introduction

Friction stir welding (FSW) is currently attracting considerable attention in the mobility industry and is seen as a promising joining technology for high-strength joints [1]. In FSW workpieces are simultaneously softened and stirred through friction between a rotating tool and the material. A schematic overview of the process is given in Fig. 1. While the tool shoulder generates heat through friction on the workpiece surface, the pin plunges into the component to stir the material. The process can be divided into three distinct phases: the initial plunge phase, during which the tool is inserted into the workpiece; the subsequent feed phase, during which forward movement of the tool begins; and finally, the plunging out phase, during which the tool is withdrawn from the workpiece.

In contrast to conventional fusion welding processes, the melting temperatures of the joining partners are not exceeded in FSW, which means that low residual stresses are generated in the material and the formation of pores and cracks can be avoided [2]. Protective gases or filler materials are not required. FSW has traditionally been used mainly for aluminium and its alloys [3].The technique is now also employed in the welding of steel, copper, magnesium, and other metals [2], including the joining of dissimilar materials [3]. Recently, the FSW of thermoplastic polymers has also attracted significant interest [4]. The process is becoming increasingly popular

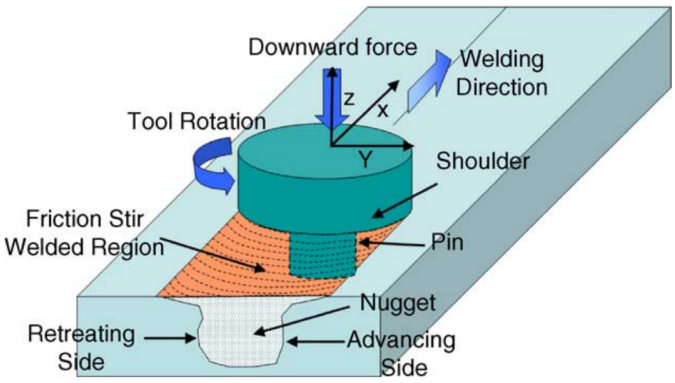

Fig. 1: Schematic overview of the friction stir welding process [1].

in modern lightweight construction, particularly due to the improved strength properties of the weld seams and the possibility of creating dissimilar joints [5].

As the process takes place below the melting temperature of the workpieces to be joined, high process forces are involved. Consequently, specialized equipment, converted milling machines [6] or parallel kinematics [7] are often used for FSW, as their high rigidity minimizes displacement of the tool and thus favors defect-free weld seams.

In contrast, serial articulated arm industrial robots (IR) are chosen due to their cost efficiency and availability, and are particularly preferable for complex weld seams due to their flexibility within the work area [8]. It has been demonstrated that IR can achieve process qualities comparable to those of conventional FSW machines [9]. To achieve this, it is essential to control the contact force acting normal to the workpiece, due to the higher compliance of the IR compared to the conventional machines [10]. This way defects in the weld seam can be prevented, which could result in an inadequate joining [11].

State-of-the-art force control structures for manufacturing with IR have a low bandwidth. While this may be sufficient for low-force processes such as grinding, it results in a reduction in achievable performance for processes with high process forces, such as robotic friction stir welding (RFSW). This paper presents a novel approach to controlling the force during RFSW in order to overcome significant limitations resulting from current low bandwidth force control structures. Firstly,

the current state of the art is presented in Sec. II. Thereafter, existing shortcomings are identified and the objectives of this research are formulated in Sec. III. Sec. IV provides an analysis of the examined control structures, which are then subjected to a comparative analysis through simulation and subsequently validated experimentally in Sec. V.

II. State of the art

The following section provides an overview of existing structures for force control in serial manipulators. Subsequently, state-of-the-art applications of force control for RFSW are summarized.

A. Force control structures

A fundamental distinction is made between an indirect and a direct approach to the force control of robots. The most prevalent example of indirect force control is impedance control, in which force outputs are computed from motion inputs [12]. In general, indirect force-controlled systems do not necessitate a closed force control loop, which is why control to a setpoint is not feasible. Since indirect force control is therefore directly influenced by the system's inherent compliance [13], this approach is not suitable for RFSW.

A variety of approaches exists for direct control of the force. However, there is no uniformity in the naming of these structures in the literature. Therefore, the most relevant structures for this research are briefly introduced and named here. The most prevalent structure in the current state of research is force control with subordinate motion control, as shown in Fig. 2, referred to in the following as *external force control*. Here, the force control loop is closed around the position control of the robot. The controller thus corresponds to a mechanical admittance. This sort of controller is used particularly frequently, as commercially available IRs typically only provide position inputs [14], whereas some collaborative robots (cobots) offer greater flexibility in the form of additional interfaces. A related but rarer form of such admittance control is created by mapping the force controller outputs to the robot's velocity interface, as demonstrated by Wahrburg et al. in their work on controlling a cobot [15]. There is no consensus in the literature regarding the definition of admittance. Some authors define it as a force-position relation, while others define it as a force-velocity relation [16]. As a result, both structures are found under the name admittance control. In this paper, the structure with an inner velocity loop will be referenced as *admittance control*.

A contrast to the introduced cascaded direct force control concepts are direct force control concepts in which the outputs of the controllers act in a parallel manner to the motion control. For example, in the hybrid position/force control structure, originally presented by Raibert and Craig in [17], additive torques are specified in parallel to the motion control. The workspace is subdivided into force-controlled and motion-controlled subspaces through the use of selection matrices. This implies that each loop controls orthogonal Cartesian subspaces; however, in joint space, each joint is simultaneously

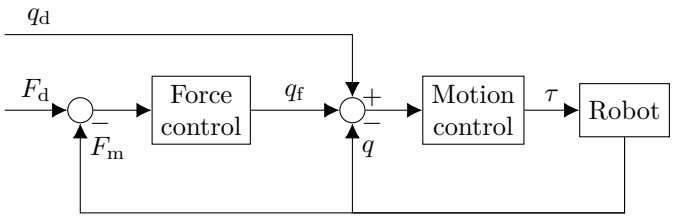

Fig. 2: Structure of the external force controller.

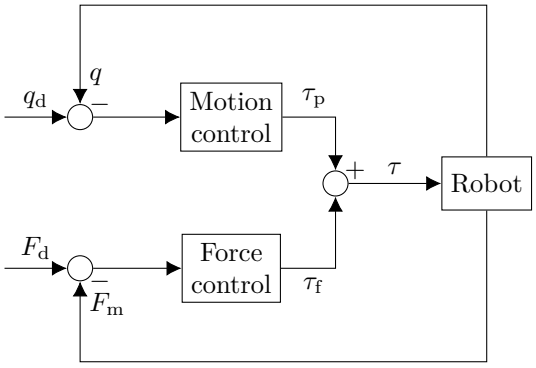

Fig. 3: Structure of the parallel force controller.

force- and position-controlled. As a result of the subdivision of the workspace, stability problems may arise if the environment is not sufficiently detailed [18]. To address this, Chiaverini developed a form of parallel force control in [19], in which the set torques calculated by the motion and force control are not decoupled but superimposed. This latter structure is shown in Fig. 3 and is referred to in the following as *parallel force control*.

B. Force control in Robotic Friction Stir Welding

In [20], Smith describes the necessity for force control in RFSW to join 3 mm aluminum sheets. External force control is employed, wherein the forces are estimated based on the motor currents. Soron replaces the contact force estimation with the measurement of the process force using a dynamometer, thereby reducing the cycle time of the control [21]. In both approaches, force control can be successfully employed during the feed phase. However, the bandwidth is insufficient to control the plunge phase, where the rate of force change is particularly high. In [22], Fehrenbacher et al. also utilize external force control to influence the plunge depth of the tool, with additional tool-side control of the process temperature. The author identifies the achieved bandwidth as the most significant performance limitation of the approach. In this case, as well, the force control is only activated after the plunge phase. The consequence of this is the necessity for the machine to be oversized in order to withstand the higher process forces that are generated during the plunge phase. In contrast, Mendes et al. also employ force control during the plunge phase in the RFSW of polymers [23]. Despite the slow plunging, an overshoot in the force profile is present, which is due to the low bandwidth of the external

force control. In [24], a simulation infrastructure is set up to optimize RFSW of aluminum for aerospace applications. In contrast to the previously mentioned approaches, the authors compare the external force control with a parallel and a hybrid force/position control using a simulated step as the desired force input. Despite the recognizable increase in bandwidth of the parallel approaches, the author decides to use external force control due to its simpler implementation and the lower overshoot observed.

III. Challenges and Objective

In the current state of the art, only external force control is used to control the contact force in RFSW. This control structure is known from other mechanical machining processes, such as grinding and polishing, where it has been used successfully for a long time [25]. However, in contrast to these processes, FSW involves significantly higher forces and force gradients [8], so a control with a wider bandwidth should be aimed for. The more complex implementation of such a structure is problematic, as often only position interfaces are available as standard for IR. However, the trend toward software-defined manufacturing and more open control systems is also evident in the robotics industry. While certain cobots already provide interfaces for specifying motor torques [26], recent developments have also seen the emergence of controller-independent robot mechanics for serial kinematics in the higher load range [27]. This suggests that there will be more opportunities in the future to implement custom control solutions on IR. It is evident that IR manufacturers already have the necessary capabilities to integrate the findings of this study into their existing systems.

By replacing the force control structure currently used in RFSW to provide more bandwidth, the following improvements seem possible:

- Improved reference tracking and disturbance rejection.
- Control of the immersion phase in which the highest force gradients occur [10]. As a result, oversizing of the system used could be avoided.
- Increasing the plunging and feeding velocity, where the bandwidth is the limiting factor [20].

In order to achieve this objective, the control of an existing ABB IRB 4400 IR is replaced by a custom control system that allows for the implementation of alternative control structures. The developed controllers are then validated and benchmarked in experiments for the plunging phase of RFSW of polycarbonate.

IV. Concept and Simulation

A. Test bench and digital twin

In order for the system to be fully customizable, the entire control cabinet is replaced. Fig. 4 illustrates a comprehensive overview of the test bench, including an outline of the surrounding control architecture. A list including the most important components is given in Tab. I. The center of the control is the Beckhoff TwinCAT real-time extension, which incorporates an integrated programmable logic controller (PLC),

TABLE I: List of components used on the test bench.

	Manufacturer	Version
Robot	ABB	IRB 4400
Drives	Bosch Rexroth	ctrlX DRIVE
Control	Beckhoff	TwinCAT 3
Safety	Pilz	PNOZmulti 2
Spindle	isel	iSA 1500 WL
FT-Sensor	Schunk	FTE-OMEGA

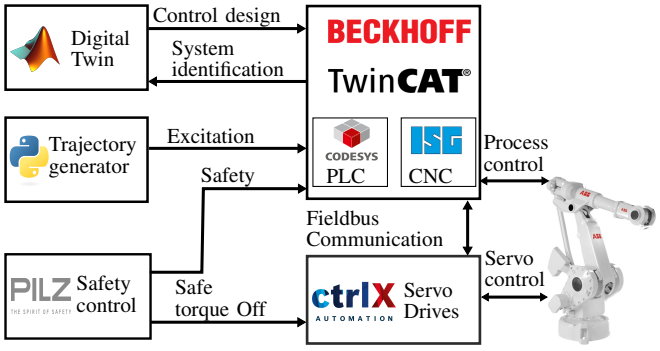

Fig. 4: Overview of the control architecture of the developed test bench.

computerized numerical control (CNC), and a human machine interface (HMI). The motors are controlled using servo drives from Bosch Rexroth, which communicate with the control via EtherCAT. Joints can be moved using either the CNC in combination with inverse kinematics or a trajectory generator for specific excitation signals like sine sweeps. The open control architecture permits the straightforward incorporation of supplementary components, such as the utilized FTE-OMEGA 6-axis force torque sensor from Schunk or the milling spindle iSA 1500 WL from isel, directly into the robot control. A digital twin, implemented in MATLAB/Simulink, is employed for system identification and the development of novel control structures. The developed control algorithms, for example force controllers or inverse kinematics, are subsequently transferred to the real-time system via code generation and the use of TwinCATs Component Object Models (TcCOM).

In order to simulate the robot with regard to its dynamic behavior, the model originally described in [29] of the form

$$M(q)\ddot{q} + C(q,\dot{q})\dot{q} + g(q) = \tau_\mathrm{g} - \tau_\mathrm{ext} \tag{1}$$

$$\tau_\mathrm{m} = J_\mathrm{m}\ddot{q} + \tau_\mathrm{f} + U^{-1}\tau_\mathrm{g} \tag{2}$$

is employed, with joint positions q, motor positions θ, the inertia matrix M, the Coriolis and centrifugal matrix C, the gravitational vector g as well as the vector of external torques τ_ext. For motor dynamics, friction τ_f, inertia J_m, and transmission ratios U are considered leading to the motor torque τ_m. The joints are modeled with flexible gearboxes, which are characterized by a stiffness K and damping D that result in the joint torque

$$\tau_g = K\left(U^{-1}\theta - q\right) + D\left(U^{-1}\dot{\theta} - \dot{q}\right). \tag{3}$$

Motion control of the joints is achieved through the use of of conventional independent joint controllers, which are industry standard [30]. They consist of position and speed controllers in a P-PI cascade. After initial manual tuning, the first three joints were subjected to robust tuning using H_{inf} synthesis and the dynamic model ((1) and (3)), as described in [31]. To enable the necessary frequency domain analysis, the joints were excited with the trajectory generator using pseudorandom binary sequences.

B. Implementation of force control

The in Sec. II-A described external and parallel force controller as well as the admittance controller are chosen for comparison and are implemented into the simulation model. The output of the external force controller is a Cartesian offset in position, which is transformed into joint space

$$q_{\mathrm{f}} = \Omega K_{\mathrm{p}} \left(e_{\mathrm{f}} + \frac{1}{T_i} \int e_{\mathrm{f}} \mathrm{d}t \right) \tag{4}$$

using inverse kinematics Ω. The controller is a standard PI-controller with the parameters K_{p} and T_{i} acting on the force error e_{f}. The joint position offset is then added to the underlying motion controllers.

In contrast to the external force controller, the parallel force controller operates in parallel with the motion control. As before, it is designed as a PI controller, where the torque offset

$$\tau_{\mathrm{f}} = J^{\intercal} K_{\mathrm{p}} \left(e_{\mathrm{f}} + \frac{1}{T_i} \int e_{\mathrm{f}} \mathrm{d}t \right), \tag{5}$$

is computed employing the concept of kineto-static duality

$$\tau_{\mathrm{ext}} = J^{\intercal}(q) h_{\mathrm{e}}, \tag{6}$$

which maps the wrench of external forces and torques h_{e} to joint space torques using the transposed manipulator Jacobian $J^{\intercal}$ [13]. The direct output of joint torques results in the bypassing of the motion control cascade, thereby increasing the bandwidth. The parallel force controller was selected over the hybrid force/position controller due to the challenge associated with providing a detailed description of the FSW environment. One example of this is the retraction of the tool at the end of the process, which results in the formation of a hole due to the ejected material. As mentioned in Sec. II-A, this lack of detail in the environment description may potentially result in stability issues when employing a hybrid control approach. It should be noted that the superimposition of motion and force control in the parallel force controller is accompanied by a reduction in bandwidth. This is attributed to the motion controller operating in opposition to the force controller. This occurs because the output of the force controller results in movement while the desired position remains constant. It is therefore essential to ensure that the force controller is the dominant control mechanism.

The output of the PI admittance controller is a joint velocity offset

$$\dot{q}_{\mathrm{f}} = J^{-1} K_{\mathrm{p}} \left(e_{\mathrm{f}} + \frac{1}{T_i} \int e_{\mathrm{f}} \mathrm{d}t \right), \tag{7}$$

which is computed using the inverse of the Jacobian J^{-1}. The output is directly added to the velocity controller input, thus bypassing the position controller in order to enhance bandwidth. In the case of cobots or other manipulators, it would be most efficient to eliminate the position controller from the structure to prevent it from working against the force controller. However, many industrial robots, including the one used for this study, have gear couplings in the front three axes. Consequently, completely eliminating the position controller would lead to unexpected behavior. Therefore, the position controller is kept as shown in the control structure in Fig. 5. Given that the position controller is strictly proportional, the counteracting behavior against the force controller is significantly less pronounced than that observed in the parallel controller.

C. Process simulation

To tune and validate the force controllers specifically for the RFSW process, experiments were conducted focusing on the plunge phase using workpieces made of polycarbonate. To assess the performance of the controllers, a process model was generated and employed. Further insights regarding the developed process model can be obtained from [28]. To clarify the significance of force control during the plunge phase, the results of the simulated position-controlled process, as well as the measured data obtained from the test bench, are presented in Fig. 6, which depicts the process force over time. The parameters utilized in this study were a plunging speed v_z of $25\,\mathrm{mm/s}$ and a spindle speed n of $1500\,\mathrm{rpm}$, which were selected based on the findings of the friction stir spot welding experiments in [32]. Both in the simulated data and in the experimental data, two distinct force peaks are visible, which are the result of the tool pin and the tool shoulder hitting the workpiece, respectively. Following these peaks is a drop in process force resulting from the heating of the workpiece. Due to effects such as tool heating, workpiece heating, and excess material welding on the tool, the process is quite volatile. As the process model was developed for a range of process parameters, discrepancies between simulated and measured data are to be expected. However, the model does accurately represent significant force peaks and increases in force, which justifies the use of the process model to initially test force controllers in simulation. The objective of controlling the force during the plunge phase is to suppress the force maxima in order to eliminate the need for oversized equipment. Furthermore, it is expected that the overall plunging time will not increase, given that the force controller is capable of accelerating the plunging speed during the softening of the material.

All PI force controllers were tuned using the process model and Matlabs Optimization Toolbox, with the main objective of minimizing the root mean squared error (RMSE). To initially assess the bandwidth of the implemented force controllers, the process model is employed in conjunction with sine sweeps of the desired force. For the parameters of the sine sweep, an offset force of $250\,\mathrm{N}$ is selected, which is subsequently superimposed by sinusoids of amplitude $50\,\mathrm{N}$ spanning a

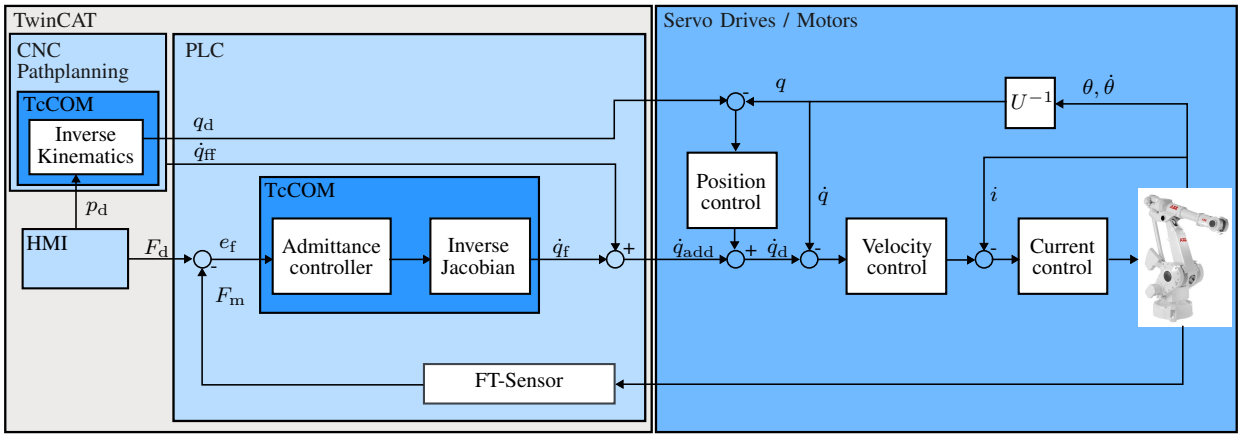

Fig. 5: Structure of the admittance controller as implemented on the test bench.

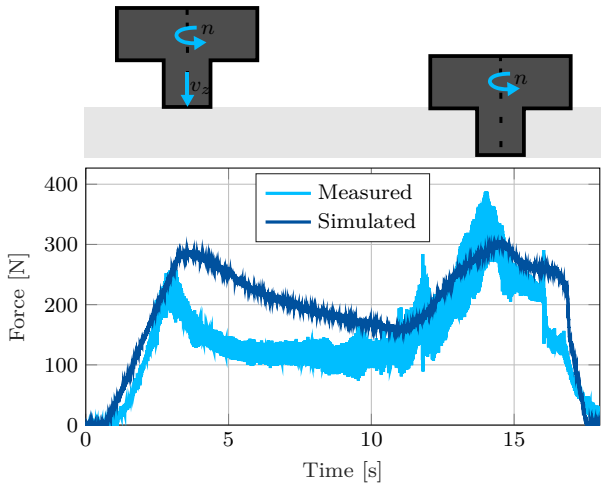

Fig. 6: Measured and simulated process force for the position controlled plunge phase.

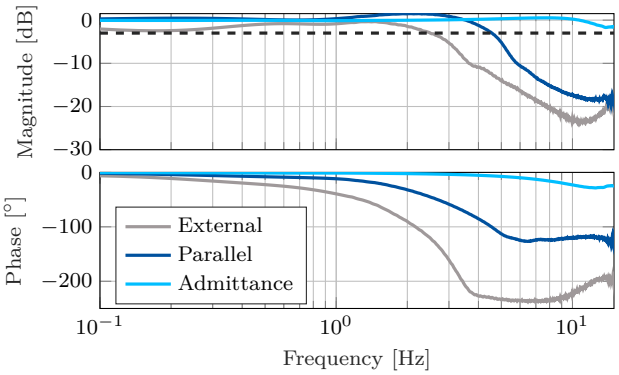

Fig. 7: Closed loop frequency response of the three implemented force controllers.

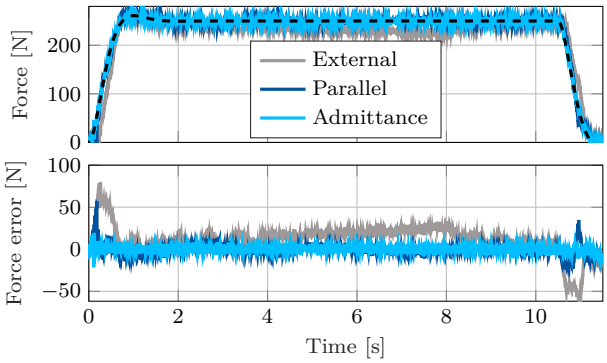

Fig. 8: Process force and force error over time during the purely force controlled plunge phase for the three controllers.

range of frequencies from 0,1 Hz to 15 Hz. Fig. 7 shows a bode plot of the closed-loop frequency response for the three force controllers. Both the parallel force controller and the admittance controller with an inner velocity loop enhance the achievable bandwidth, indicated by the dashed line at -3 dB magnitude, in comparison to the external force controller utilized in the state of the art. Although the parallel force controller represents the most direct approach and circumvents the delays introduced by the underlying motion control cascade, the bandwidth improvement is less pronounced than with the admittance controller. This is due to the integrators of velocity and force control operating in opposition to one another.

The difference in bandwidth is reflected in the process simulation of the purely force controlled plunge phase, in the absence of an additional position trajectory. The desired force is a profile resulting from filtering the desired steady state force of 250 N with a digital biquad filter. Fig. 8 depicts the process force, along with the force error over time for the three controllers. The dashed line represents the desired force profile. The initial force error resulting from the gap between the tool and the workpiece at the start of the process demonstrates the enhanced reaction time of the higher bandwidth controllers. A similar phenomenon is observed when the workpiece undergoes softening as a consequence of the friction-induced heating. The low bandwidth external force controller is unable to track the desired force, which, at a higher scale, could result in inadequate welding and defects in the seam.

In a standard FSW process the plunge phase ends with

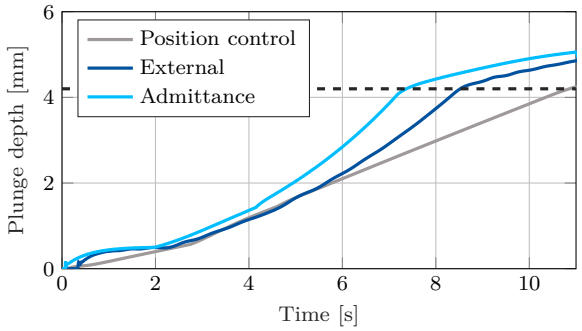

Fig. 9: Plunge depth over time for the admittance controller, the external force controller, and the position controller.

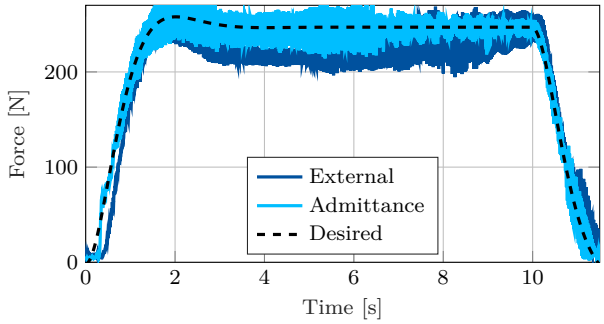

Fig. 10: Experimental validation of the process force and force error over time.

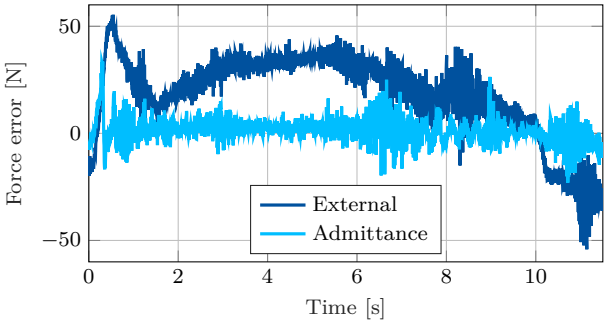

Fig. 11: Notch filtered force error over time.

the tool shoulder exerting pressure on the workpiece. After that the feed motion begins. As anticipated, the introduction of force control during the plunge phase does not result in an increase in the overall duration of the phase. Instead, it leads to a reduction in the overall time, as illustrated in Fig. 9, which depicts the plunge depth over time. The dashed line indicates contact of the tool shoulder, which is reached earliest by the high bandwidth admittance controller due to the acceleration during softening. Compared to the position controller, the plunge time decreases by $32\,\%$, while compared to the external force controller, a reduction of $14\,\%$ is achieved. As the parallel force controller is found to be less effective than the admittance controller, only the latter is subjected to validation on the test bench and compared against the external force controller.

V. Experimental Validation

As described in Sec. IV, the admittance controller is ported to the TwinCAT controller using MATLAB code generation and the implementation via TcCOM. This allows for the controller to be integrated in the PLC, as shown in Fig. 5, communicating to the servo drives over EtherCAT at a rate of $1\,\mathrm{kHz}$, while the underlying motion control is computed on the servo drives. The velocity offset calculated by the admittance controller is incorporated into the velocity feedforward $\dot{q}_{\mathrm{ff}}$ from the CNC and communicated as an additional velocity input $\dot{q}_{\mathrm{add}}$ to the velocity controller.

In this study, the force-controlled plunging phase was analyzed utilizing a workpiece of $6\,\mathrm{mm}$ thick polycarbonate. The controller and process parameters were set in accordance with the simulation (see Sec. IV-C). The selected admittance controller with inner velocity loop is compared to the state-of-the-art external force controller in Fig. 10, which depicts the process force over plunging time. The discrepancy between the simulation results and the actual outcome is primarily attributed to unmodeled process noise. After applying a fast Fourier transform (FFT) to the signal, the responsible frequency was found to be $50\,\mathrm{Hz}$, which is equivalent to half a rotation of the tool. In Fig. 11, which depicts the force error over time, this frequency is filtered using a notch filter. This confirms the key findings from the process simulation. In comparison, the external force controller yielded a RMSE of $26{,}85\,\mathrm{N}$, in contrast to the $5{,}83\,\mathrm{N}$ obtained with the admittance controller. This represents an increase in accuracy of $78\,\%$. In general, the admittance controller enables more effective and efficient tracking of the desired force.

VI. Conclusion

This paper presents a novel approach to force control for robotic friction stir welding. Instead of closing the force control loop in cascade above the motion control, a parallel structure and an admittance controller with inner velocity loop were implemented and analyzed. To this end, an industrial robot with an open control architecture was utilized, allowing for comprehensive access to the robot controllers. A process model of the critical plunge phase for the robotic friction stir welding of polycarbonate workpieces was employed to initially assess the efficacy of the implemented controllers in a digital twin. It was demonstrated that the lack of bandwidth of the state-of-the-art external force controller results in inadequate and delayed reference tracking, which could potentially lead to defects in the resulting weld seams. The implemented admittance controller with an inner velocity loop demonstrated a notable enhancement in bandwidth, which led to enhanced reference tracking and a higher plunging speed. The simulated findings were validated on the test bench, exhibiting an increase in accuracy of $78\,\%$.

Acknowledgment

The authors would like to thank the Federal Ministry for Economic Affairs and Climate Action (BMWK) for funding

the joint project: SDM4FZI as part of the “Future Investments in the Automotive Industry” funding program.

REFERENCES

[1] R. S. Mishra and Z. Y. Ma, ”Friction stir welding and processing,” Materials Science and Engineering: R: Reports, vol. 50, 1-2, pp. 1–78, 2005, doi: 10.1016/j.mser.2005.07.001.

[2] P. Gebhard, Dynamisches verhalten von werkzeugmaschinen bei anwendung für das rührreibschweißen: Herbert Utz Verlag, 2011.

[3] A. Roth, Modellierung des Rührreibschweißens unter besonderer Berücksichtigung der Spalttoleranz: Herbert Utz Verlag, 2017.

[4] A. Zafar, M. Awang, and S. R. Khan, ”Friction stir welding of polymers: An overview,” in 2nd international conference on mechanical, manufacturing and process plant engineering, pp. 19–36.

[5] M. Werz, Experimentelle und numerische Untersuchungen des Rührreibschweißens von Aluminium-und Aluminium-Stahl-Verbindungen zur Verbesserung der mechanischen Eigen-schaften: Materialprüfungsanstalt (MPA), Universität Stuttgart, 2020.

[6] N. Mendes, P. Neto, A. Loureiro, and A. P. Moreira, ”Machines and control systems for friction stir welding: A review,” Materials & Design, vol. 90, pp. 256–265, 2016, doi: 10.1016/j.matdes.2015.10.124.

[7] J. Xiao, M. Wang, H. Liu, S. Liu, H. Zhao, and J. Gao, ”A constant plunge depth control strat-egy for robotic FSW based on online trajectory generation,” Robotics and Computer-Integrated Manufacturing, vol. 80, p. 102479, 2023, doi: 10.1016/j.rcim.2022.102479.

[8] J. de Backer, Feedback control of robotic friction stir welding: University West, 2014.

[9] M. F. Zaeh and G. Voellner, ”Three-dimensional friction stir welding using a high payload in-dustrial robot,” Prod. Eng. Res. Devel., vol. 4, 2-3, pp. 127–133, 2010, doi: 10.1007/s11740-009-0184-y.

[10] G. E. Cook, R. Crawford, D. E. Clark, and A. M. Strauss, ”Robotic friction stir welding,” Indus-trial Robot: An International Journal, vol. 31, no. 1, pp. 55–63, 2004, doi: 10.1108/01439910410512000.

[11] W. R. Longhurst, Force control of friction stir welding: Vanderbilt University, 2009.

[12] N. Hogan, ”Impedance Control: An Approach to Manipulation,” in 1984 American Control Conference, San Diego, CA, USA, 1984, pp. 304–313.

[13] B. Siciliano, Robotics. London: Springer London, 2009.

[14] C. Ott, Cartesian Impedance Control of Redundant and Flexible-Joint Robots. Berlin, Heidel-berg: Springer Berlin Heidelberg, 2008.

[15] A. Wahrburg, J. Bös, K. D. Listmann, F. Dai, B. Matthias, and H. Ding, ”Motor-current-based estimation of cartesian contact forces and torques for robotic manipulators and its application to force control,” IEEE Transactions on Automation Science and Engineering, vol. 15, no. 2, pp. 879–886, 2017.

[16] M. Schumacher, J. Wojtusch, P. Beckerle, and O. von Stryk, ”An introductory review of active compliant control,” Robotics and Autonomous Systems, vol. 119, pp. 185–200, 2019, doi: 10.1016/j.robot.2019.06.009.

[17] M. H. Raibert and J. J. Craig, ”Hybrid Position/Force Control of Manipulators,” Journal of Dy-namic Systems, Measurement, and Control, vol. 103, no. 2, pp. 126–133, 1981, doi: 10.1115/1.3139652.

[18] S. Chiaverini and L. Sciavicco, ”The parallel approach to force/position control of robotic manipulators,” IEEE Transactions on Robotics and Automation, vol. 9, no. 4, pp. 361–373, 1993.

[19] S. Chiaverini and L. Sciavicco, ”Force/Position Control of Manipulators in Task Space with Dominance in Force,” IFAC Proceedings Volumes, vol. 21, no. 16, pp. 137–143, 1988, doi: 10.1016/S1474-6670(17)54600-5

[20] C. B. Smith, ”Robotic friction stir welding using a standard industrial robot,” Kei Kinzoku Yosetsu(Journal of Light Metal Welding and Construction), vol. 42, no. 3, pp. 40–41, 2004.

[21] M. Soron and I. Kalaykov, ”A robot prototype for friction stir welding,” in 2006 IEEE Confer-ence on Robotics, Automation and Mechatronics, pp. 1–5.

[22] A. Fehrenbacher, C. B. Smith, N. A. Duffie, N. J. Ferrier, F. E. Pfefferkorn, and M. R. Zinn, ”Combined temperature and force control for robotic friction stir welding,” Journal of manufac-turing science and engineering, vol. 136, no. 2, 2014.

[23] N. Mendes, P. Neto, M. A. Simão, A. Loureiro, and J. N. Pires, ”A novel friction stir welding robotic platform: welding polymeric materials,” The International Journal of Advanced Manu-facturing Technology, vol. 85, pp. 37–46, 2016.

[24] A. Bres et al., ”Simulation of friction stir welding using industrial robots,” Industrial Robot: An International Journal, vol. 37, no. 1, pp. 36–50, 2010, doi: 10.1108/01439911011009948.

[25] F. Chen, H. Zhao, D. Li, L. Chen, C. Tan, and H. Ding, ”Contact force control and vibration suppression in robotic polishing with a smart end effector,” Robotics and Computer-Integrated Manufacturing, vol. 57, pp. 391–403, 2019, doi: 10.1016/j.rcim.2018.12.019.

[26] Franka Emika, Franka Control Interface Documentation. [Online]. Available: https://frankaemika.github.io/docs/index.html

[27] Autonox Robotics, Homepage. [Online]. Available: https://www.autonox.com/de

[28] V. Kamm, P. Mesmer, A. Lechler, and A. Verl, ”Prozessmodellierung für das Rührreibschweißen/Process modeling of friction stir welding – Semi-analytical process model of robotic friction stir welding,” wt, vol. 113, no. 05, pp. 183–188, 2023, doi: 10.37544/1436-4980-2023-05-5.

[29] Spong, M. W. (1987): Modeling and Control of Elastic Joint Robots. In: Journal of Dynamic Systems, Measurement, and Control 109 (4), S. 310–318. DOI: 10.1115/1.3143860.

[30] Albu-Schäffer, Alin: Regelung von Robotern mit elastischen Gelenken am Beispiel der DLR-Leichtbauarme. München, Techn. Univ., Diss., 2002.

[31] Mesmer, Patrick; Neubauer, Michael; Lechler, Armin; Verl, Alexander (2022): Robust design of independent joint control of industrial robots with secondary encoders. In: Robotics and Computer-Integrated Manufacturing 73, S. 102232. DOI: 10.1016/j.rcim.2021.102232.

[32] A. Paoletti, F. Lambiase und A. Di Ilio, ”Analysis of forces and temperatures in friction spot stir welding of thermoplastic polymers“, The International Journal of Advanced Manufacturing Technology, Jg. 83, Nr. 5, S. 1395–1407, 2016.